OPEN ACCESS

Electrodeposition of Equiatomic FePt Permanent Magnets from Non-Aqueous Electrolytes Based on Ethylene Glycol

Journal of The Electrochemical Society, 2022 **169** 072506

Electrodeposition of Equiatomic FePt Permanent Magnets from Non-Aqueous Electrolytes Based on Ethylene Glycol

Roberto Bernasconi,[1,*,z] Anna Nova,[1] Salvador Pané,[2] and Luca Magagnin[1,*]

[1]*Dipartimento di Chimica, Materiali e Ingegneria Chimica "Giulio Natta," Politecnico di Milano, Via Mancinelli 7, 20131, Milano, Italy*
[2]*Multi-Scale Robotics Lab, Institute of Robotics and Intelligent Systems, ETH Zurich, Tannenstrasse 3, CH-8092, Zürich, Switzerland*

The highly ordered $L1_0$ hard-magnetic phase of the equiatomic FePt alloy is of significant interest for a great number of applications, ranging from the realization of magnetic sensors to the deposition of thin layers for vertical recording. In this context, the development of wet deposition processes able to yield high-quality layers of FePt represents a need of considerable industrial relevance. While several aqueous-based electrodeposition approaches have been developed for the manufacturing of FePt, these formulations evidenced substantial technological limitations, specifically connected to the use of water as solvent. The present work describes the deposition of FePt from a non-aqueous electrolyte based on ethylene glycol, which presents potential advantages in terms of gas evolution reduction and purity improvement of the obtained coatings. Deposition was carried out using Fe(III) and Pt(IV) as precursors and ammonium chloride as additive to enhance the quality of the coatings and their compositional uniformity. In this way, equiatomic FePt thin films characterized by a good morphology were easily obtained. After annealing at 600 °C, their microstructure changed and the disordered fcc phase present in the as-plated alloy evolved into the highly magneto-crystalline anisotropic $L1_0$ phase. As a consequence, coercivity reached values in excess of 10 kOe.
 [DOI: 10.1149/1945-7111/ac81f8]

Manuscript submitted May 9, 2022; revised manuscript received July 4, 2022. Published July 28, 2022.

Supplementary material for this article is available online

Among the family of hard-magnetic materials, equiatomic FePt results to be a promising material for many applications. In particular, the $L1_0$ ordered phase with face-centred-tetragonal structure (fct) is the one presenting the properties of interest. It is hard ferromagnetic, with a high saturation magnetization and a large remanent magnetization. It is also characterized by a relatively high Curie temperature, equal to 650 K, and by a good chemical stability against oxidation.[1] These properties make $L1_0$ FePt interesting for applications such as micro-magnets in micro-electromechanical systems (MEMS).[2,3] Its magneto-crystalline anisotropy, based on 3d and 5d electrons, is considerably high (the uniaxial anisotropy constant K_u reaches 6.6–10×10^7 erg cm^{-2}). This is due to the large spin–orbit coupling in the 5d-element and allows for thermally stable grain size down to ≃3 nm.[4,5] $L1_0$ FePt could be therefore successfully employed in ultra high-density recording media.[6,7] Another feature of this material that results worth of attention is its biocompatibility that allows its employment in biomedical devices such as small-scale robots. FePt, indeed, has been demonstrated to be nonimmunogenic, noncytotoxic and hemocompatible.[8] For example, Kadiri et al. realized magnetically actuated helical microdevices by incorporating small amounts of FePt in their microstructures.[9]

FePt has been prepared by a variety of methods including pulsed laser deposition,[10] vapor deposition[11] and high-vacuum magnetron-sputtering.[12] Electrodeposition, however, is a viable alternative, which allows to obtain, in a simple and cost-effective way, thick and continuous films on substrates with any shape. Generally, the as-deposited FePt is constituted by the fcc phase and is magnetically soft. In order for the desired $L1_0$ hard ferromagnetic fct phase to develop, an annealing step is required. Thongmee et al. deposited FePt from an aqueous bath and performed annealing for 20 min in a H_2–Ar (5% vol H_2) mixed atmosphere.[13] Depending on the substrate, the temperature that allowed to reach the highest coercivity varied: on gold the best result was 10000 Oe after annealing at 600 °C, on silver 18000 Oe after annealing at 800 °C and on copper 4000–5000 Oe after annealing at 600 °C. At longer annealing times or at higher temperatures the amount of $L1_0$ phase formed increases, therefore also the coercivity of the treated deposit results higher. The maximum value of coercivity obtained by S. Ichihara et al. by postannealing in H_2 at the relatively low temperature of 400 °C was indeed 6000 Oe.[14] Rhen et al. annealed their electrodeposited FePt layers at 900 °C for 2 h and achieved a value of coercivity equal to 15000 Oe.[15] A coherent result was obtained by Leistner et al., who achieved a coercivity of 11000 Oe by annealing at 600 °C in H_2 atmosphere for 10 min.[2]

Water is usually the preferred solvent for electroplating baths thanks to its high versatility and low cost. Yet, its use involves hydrogen evolution to leaser or a larger extent. This can result in hydrogen embrittlement phenomena and in the passivation of the cathode, hindering the fabrication of thick and compact metallic coatings. Furthermore, hydrogen evolution causes a reduction of current efficiency. Aqueous baths present also problems related to thermal instability and even at low temperatures are subjected to evaporation.[16] Finally, their use in electrodeposition leads to a high content of oxygen in the deposits in the form of oxides and hydroxides, compounds that lower the purity level of the final layer. Therefore, non-aqueous electrolytes represent a promising alternative for the electrosynthesis of metallic layers. They can be classified into two categories: ionic liquids[17] and organic solvent-based electrolytes. Ionic liquids are salts with a melting temperature below 100 °C and they present a wide potential window and a high solubility of metal salts. In particular, eutectic based ionic liquids are described by the following general formula $R_1R_2R_3R_4N^+$ X. z Y, where $R_1R_2R_3R_4N^+$ is a cation, like for example $HOC_2H_4N^+(CH_3)_3$, X is generally a halide anion, Y is a Lewis or Brønsted acid and z represents the number of Y molecules that complex X^-. These compounds, called deep eutectic solvents, are simple to prepare, formulated from relatively cheap components, almost unreactive with water and, in most cases, biodegradable.[16,18] Thanks to these properties, they have been employed for the electrodeposition of metals, like silver,[19] ruthenium,[20] indium,[21] tin,[22] zinc,[23,24] copper[25] and cobalt;[26] of metallic alloys, like SnBi,[27] SmCo,[28] SnCuNi,[29] PdAg,[30] NdFe[31] and CuZn;[32] of composites, like NiSn-reduced graphene oxide,[33] Ni-TiO_2,[34] Ni-cerium molybdenum oxide hydrate microflakes,[35] Ni-nano sized SiC[36] and nanosized cobalt oxy-hydroxide.[37]

Organic solvents include for example acetone, ethanol ethylene carbonate, ethylene glycol, propylene carbonate and ethylenediamine

*Electrochemical Society Member.
[z]E-mail: roberto.bernasconi@polimi.it

dihydrochloride.[38] Concerning the electroplating of equiatomic FePt from non-aqueous baths, ethylene glycol seems to be the preferred solvent. This organic compound has been successfully employed also in other electroplating processes, including the deposition of ZnNi Alloys[39] and of nanostructured iron films.[40] Its use in FePt electroplating has been introduced by Hong-ru et al., who employed ammonium hexachloroplatinate ($(NH_4)_2PtCl_6$) and iron dichloride ($FeCl_2$) in a solution based on ethylene glycol (EG) and 1-Ethyl-3-methylimidazolium chloride (EMIC).[41] Subsequently, they electrodeposited FePt nanowires on Si(111) from an electrolyte with the same composition.[42]

In our work, we have developed a new process for FePt electrodeposition from an ethylene glycol-based bath. To provide iron ions to the electrolyte, the $FeCl_3$ salt was selected. In this way, iron was dissolved as Fe(III), which cannot be further oxidized. However, in aqueous environments Fe^{3+} ions show the tendency to be hydrolysed, leading to the precipitation of hydroxides.[43] Indeed, Cherevko et al. introduced the use of ammonium citrate in order to stabilize the electrolyte.[44] In our case, instead, the content of water in the bath resulted to be low, so the solution was intrinsically more stable and we were able to store it for few months without the occurrence of degradation issues. The effect of the NH_4Cl additive on the electrodeposition behaviour was also investigated. This compound increases the bath conductivity and modifies the composition of the plated alloy. Its use has already been documented for ZnNi deposition from choline chloride-based ionic liquids.[45] Finally, an annealing step was performed at 600 °C for 1 h under reducing atmosphere (5% vol H_2). The resulting FePt layers were characterized in terms of morphology, magnetic properties and phase composition.

Experimental Methods

Materials.—In order to prepare the electroplating bath, ethylene glycol ($C_2H_6O_2$; from Sigma-Aldrich; purity 99.8%; declared water content $\leqslant$ 0.003%), potassium hexachloroplatinate (K_2PtCl_6; from Sigma-Aldrich; purity 98%), iron (III) chloride ($FeCl_3$; from Sigma-Aldrich; purity $\geqslant$ 98%) and ammonium chloride (NH_4Cl; from Sigma-Aldrich; purity $\geqslant$ 99.5%) were employed.

Electrolytes preparation and FePt deposition tests.—Fe and Pt salts were dissolved in EG varying their concentration respectively between 20 and 50 mM and between 2 and 20 mM. The influence of NH_4Cl in solution was evaluated by changing the ratio between the molar concentration of NH_4Cl and the molar concentration of metal salts. Four different ratios were tested: 1, 2, 2.5 and 3. During the preparation of the electrolyte, the deposition process and the electrochemical characterization, the temperature was kept at the constant value of 70 °C by use of a hotplate controlled by a thermocouple. Substrates were obtained by cutting silicon wafers covered with a 20 nm Pd + 100 nm Au multilayer and, subsequently, by degreasing their surface with an ultrasonic bath of 5 min in acetone. The electroplating process was carried out working in potential control; in particular, a standard three-electrode cell setup was employed and a range of potentials going from −1400 to −2200 mV was tested. The cathode consisted of the substrate to be plated, the anode of a mixed oxides coated Ti grid and the reference electrode of a platinum wire. Deposition time was varied between 1800 and 10800 s. The potentiostat employed was an AMEL2550 potentiostat-galvanostat.

Electrochemical characterization.—The electrochemical characterization of the electrolyte was carried out by performing cyclic voltammetry (CV) at different scan rates: 20, 50 and 100 mV s^{-1}. Pt was used as reference electrode, the silicon wafer covered with the 20 nm Pd + 100 nm Au multilayer was used as working electrode and a mixed oxides coated Ti grid was used as counter electrode. The potentiostat employed was an AMEL2550 potentiostat-galvanostat.

FePt anneling procedure.—In order for the deposited FePt alloy to develop the desired hard ferromagnetic behaviour, an annealing step was necessary. Therefore, some samples were annealed in a Carbolite tubular oven for 1 hour under a H_2 atmosphere (5% vol H_2 and remaining N_2). The temperature was set at 600 °C.

Characterization techniques.—Scanning electron microscopy (SEM) was performed using a Zeiss EVO 50 EP setup equipped with an energy dispersive spectroscopy (EDS) module (Oxford instruments INCA). XRD characterization was carried out using a Philips PW1830 (Kα1Cu = 1.54058 Å). X-ray fluorescence spectroscopy (XRF) was performed using a Fischerscope X-ray XAN. AFM measurements were acquired using a NT-MDT Solver Pro. Roughness values were extracted from the AFM data acquired. Vibrating sample magnetometry (VSM) was carried out at room temperature using a Princeton Measurement Corporation MicroMag 3900. The applied magnetic field was varied between −22500 and 22500 Oe. Acquisition step size was set to 2500 Oe between −22500 and −10000 Oe, to 1000 Oe between −10000 and −2000 Oe, to 200 Oe between −2000 and 2000 Oe, to 1000 Oe between 2000 and 10000 Oe, to 2500 Oe between 10000 and 22500 Oe. Conductivity of the electrolytes was measured using an AMEL model 2131 conductivity meter. Viscosity was investigated using a Haake Viscotester VT5R rotational viscometer. Water content of the electrolytes was evaluated performing Karl Fischer titration with a Metrohm 870 KF Titrino Plus.

Data repeatability.—The electrodeposition experiments and the characterization tests were repeated at least twice to evaluate repeatability. No significant deviations from the data presented were observed.

Results and Discussion

Electrolytes water content.—In case of non-aqueous electrolytes, it is important to determine the water content, since it considerably affects the electroplating process in terms of behaviour of the metallic ions present in the bath[25,46] or it varies the potential window of the electrolyte.[47] Therefore, Karl Fischer titration was performed on two newly prepared solutions with the compositions reported in Table I. The values reported in the same table were obtained by averaging the results of three separate measures.

According to the manufacturer, the EG employed was characterized by a small level of water contamination ($\leqslant$0.003% wt). As expectable, despite the fact that no hydrated salts were employed, additional water was incorporated in the electrolyte when $FeCl_3$ and K_2PtCl_6 were added. The use of NH_4Cl as additive further increased the amount of water present in the electrolyte, from 0.14% wt to 0.21% wt. Globally, however, the amount of water in the solution resulted to be small, especially if compared to other moisture-stable non-aqueous electrolytes reported in literature. For example, water

Table I. Results of the Karl Fischer titration.

Solution	$FeCl_3$ [mM]	K_2PtCl_6 [mM]	NH_4Cl [mM]	H_2O [% wt]
1	40	20	0	0.14 ± 0.02
2	40	20	120	0.21 ± 0.02

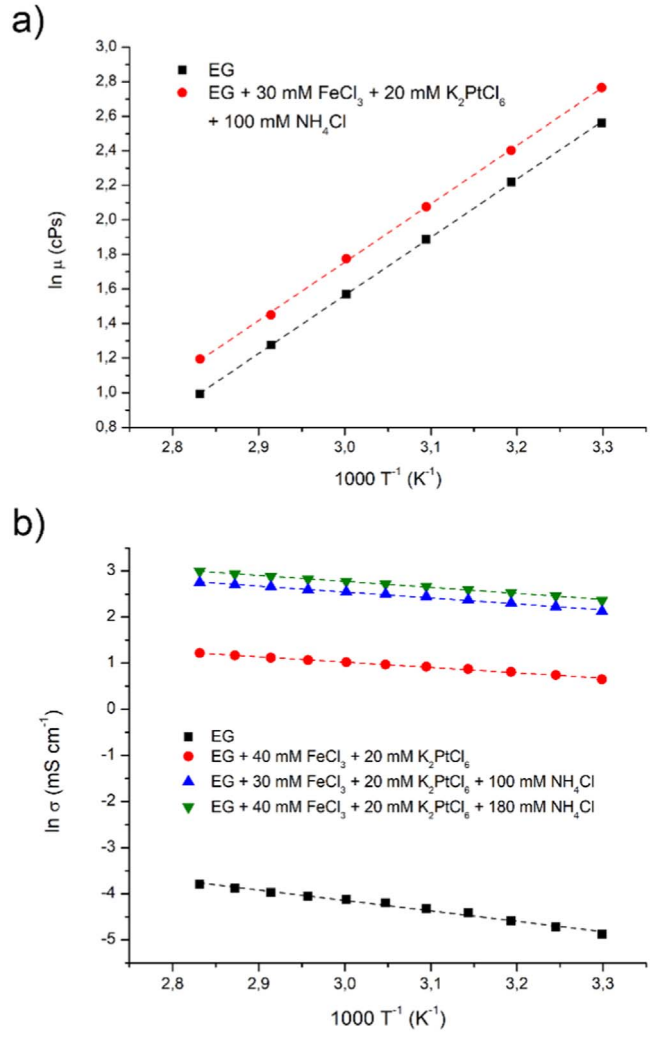

Figure 1. Viscosity (a) and conductivity (b) at different temperatures of pure EG and of EG-based electrolytes containing K_2PtCl_6, $FeCl_3$ or NH_4Cl.

contamination in excess of 1% wt has been reported for choline chloride based deep eutectic solvents additivated with hydrated metal salts.[39,46]

Electrolytes physical characterisation.—In the case of non-aqueous solutions, it is important to characterize the physical properties of the electrolytes prior to electrodeposition. In particular, viscosity and the conductivity must be carefully determined with respect to the working temperature of the electrolyte. Indeed, the two are strictly correlated by the Walden relationship, which predicts that molar conductivity decreases when dynamic viscosity increases.[48] Moreover, conductivity increases with temperature according to Eq. 1.[49]

$$\ln \quad \sigma_T = \ln \quad \sigma_0 - \quad \frac{E_\sigma}{RT} \qquad [1]$$

σ_T is the conductivity at temperature T, σ_0 is the conductivity at a reference temperature and E_σ is the activation energy for conduction. In contrast, viscosity decreases when the temperature increases (as described by Eq. 2).[49]

$$\ln \quad \mu_T = \ln \quad \mu_0 + \quad \frac{E_\eta}{RT} \qquad [2]$$

μ_T is the viscosity at temperature T, μ_0 is the viscosity at a reference temperature and E_η is the activation energy for viscous flow. Both viscosity and conductivity play a fundamental role in electrodeposition and must be carefully controlled by varying the temperature of the electrolyte or by its additivation with dissolved salts. As a matter of fact, too high viscosity results into reduced ionic mobility, which translates into poor mass transport towards the surface. Low conductivity, in turn, results into reduced power efficiencies and problematic layer formation.[50]

Both viscosity and conductivity were measured at different temperatures for some selected electrolytes described in the present work and the results are reported in Fig. 1. Raw data are reported in Figs. S1 and S2 (available online at stacks.iop.org/JES/169/072506/mmedia), while Fig. 1 reports the linearization performed according to the relationships visible in Eqs. 1 and 2 (logarithm of viscosity/conductivity vs inverse of temperature).

Concerning the viscosity, the most relevant consideration extrapolated from the data reported in Fig. 1a is the limited effect of salts. The viscosity of EG alone is only slightly lower than the values recorded for the electrolyte containing 20 mM K_2PtCl_6, 30 mM $FeCl_3$ and 100 mM NH_4Cl. In general, viscosity was relatively low and comparable with water-based solutions at temperatures higher than 50 °C. As shown in Fig. 1a, the experimental data displayed a good linearity. The activation energy for viscous flow, E_η, was determined and it resulted equal to 27.98 ± 0.11 kJ mol^{-1} for pure EG and to 28.06 ± 0.25 kJ mol^{-1} for the salts containing solution.

Considering conductivity, the most important observation regards the addition of NH_4Cl to the solution, which significantly increased the conductivity of the electrolytes. The effect is clear by looking at Fig. 1b. As expectable, the conductivity of pure EG was extremely low. EG, contrarily to deep eutectic solvents like the ones based on choline chloride, is a virtually non-dissociated diol containing no free ions. As already observed,[39,40] the addition of dissociable salts like K_2PtCl_6 and $FeCl_3$ provided ions in the solution, increasing the conductivity of many orders of magnitude and making it suitable for electrodeposition. The further addition of a relatively low quantity of NH_4Cl, however, produced a remarkable effect on the conductivity of the solution. In particular, it increased by two orders of magnitude, reaching levels comparable to choline chloride-based deep eutectic solvents.[49] This is indicative of a very high dissociation for NH_4Cl in EG, resulting in a high availability of ions able to conduct electricity. As for viscosity, the experimental data obtained for conductivity were characterized by a good linearity (Fig. 1b). The activation energy for conduction, E_σ, was determined and it resulted equal to 18.78 ± 0.67 kJ mol^{-1} for pure EG, to 9.65 ± 0.22 kJ mol^{-1} for the 20 mM K_2PtCl_6 + 50 mM $FeCl_3$ electrolyte, to 10.75 ± 0.28 kJ mol^{-1} for the 20 mM K_2PtCl_6 + 30 mM $FeCl_3$ + 100 mM NH_4Cl electrolyte and to 10.82 ± 0.20 kJ mol^{-1} for the 20 mM K_2PtCl_6 + 40 mM $FeCl_3$ + 180 mM NH_4Cl electrolyte.

Operative conditions for FePt electrodeposition were determined by considering the data obtained from viscosity and conductivity characterization. In particular, in order to minimize viscosity and to maximize conductivity, a relatively high working temperature was selected (70 °C). At this temperature, for example, the 20 mM K_2PtCl_6 + 30 mM $FeCl_3$ + 100 mM NH_4Cl was characterized by a conductivity equal to 14.21 mS cm^{-1} and a viscosity equal to 4.26 cPs.

Electrolytes electrochemical characterisation.—The electrochemical characterisation of the electrolyte was performed through cyclic voltammetry. In order to better examine the behaviour of the single metallic species, separate voltammetic scans in a solution of K_2PtCl_6 and in a solution of $FeCl_3$ were carried out. High scan rates (50 and 100 mV s^{-1}) were preferred to highlight the anodic and cathodic peaks.

The solution of K_2PtCl_6 consisted in 100 ml of ethylene glycol with a concentration of 2 mM of the salt. Figure 2a shows the voltammetries performed on this solution. The curves associated to the negative scan showed a first reduction starting at −0.2 V vs Pt (E_{onset}), which corresponded to the reduction of Pt(IV) to Pt(II),[51] and a second one, with E_{onset} = −0.8 V vs Pt and E_{peak} = −1.25 V

vs Pt, indicating the reduction of Pt(II) to metallic platinum. In the positive scans an oxidation peak, corresponding to the transition from Pt(0) to Pt(II), appeared with $E_{onset} = -0.95$ V vs Pt and $E_{peak} = -0.3$ V vs Pt. Instead, the presence of another peak at around -1.25 V vs Pt seems to be related to hydrogen desorption from Pt.[52] The presence of this peak suggests the occurrence of a parasitic hydrogen evolution reaction during the cathodic sweep, which was realistically caused by the water impurities introduced in the solution with the platinum salt. The main detected features of this voltammetric analysis match those highlighted in literature. For example, Gómez et al. observed (on Pt as substrate in a choline chloride + urea deep eutectic solvent containing Na_2PtCl_6) a first reduction peak reaching its maximum around -0.12 V vs Pt during the negative scan, followed by a second peak starting at -1.05 V vs Pt. Considering the positive scan, they identified an oxidation peak at -0.49 V vs Pt.[53] In our case, the cathodic and the corresponding anodic peak resulted to be separated by a large potential interval. This aspect can be explained considering the high viscosity and low conductivity of the non-aqueous solvent. Furthermore, the shapes of the corresponding cathodic and anodic peaks are asymmetrical and

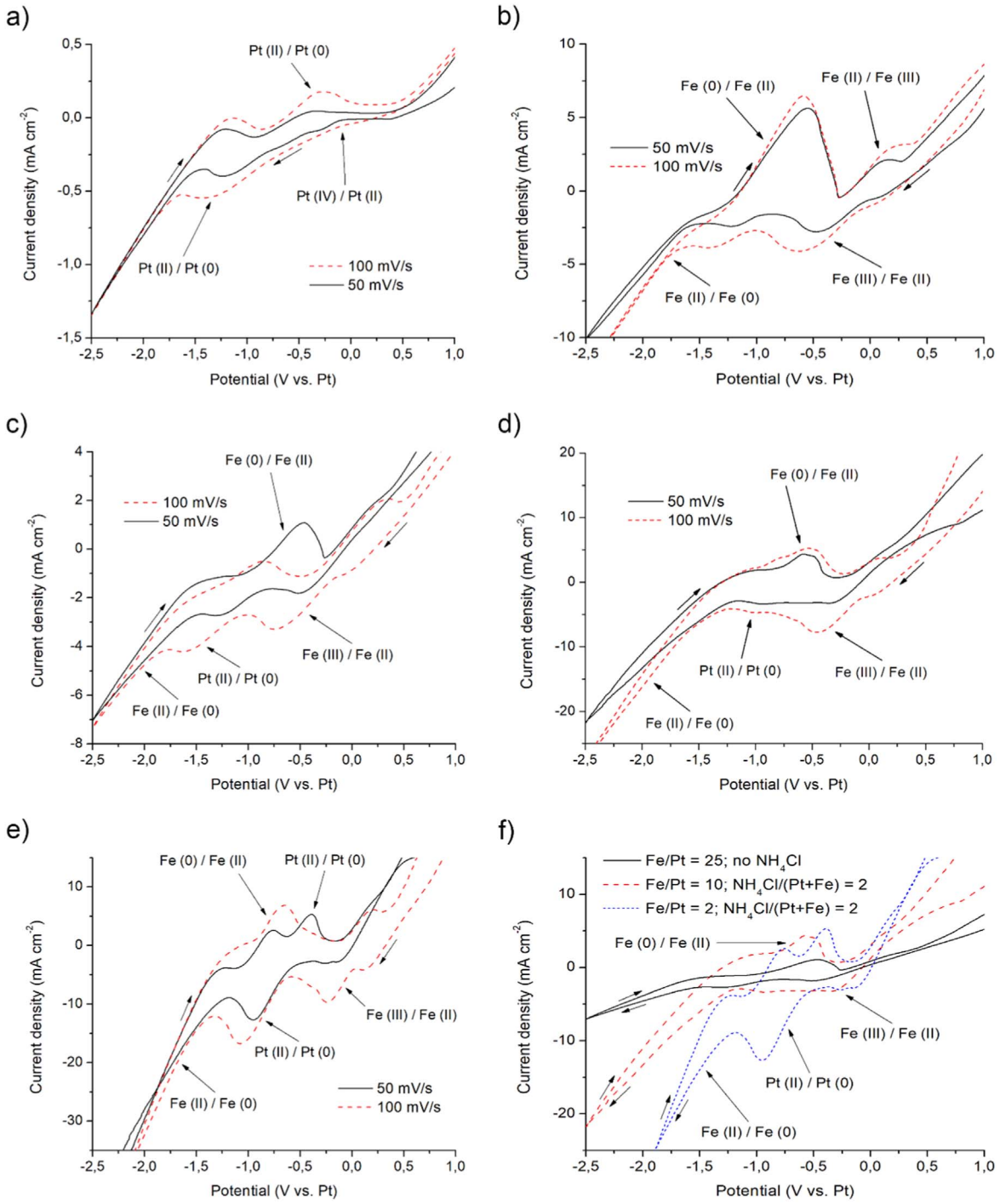

Figure 2. Voltammetries of EG-based electrolytes containing 2 mM K_2PtCl_6 (a), 50 mM $FeCl_3$ (b); voltammetries of the FePt EG-based electrolyte with ratio Fe/Pt = 25 and no NH_4Cl (c); voltammetries of the FePt EG-based electrolyte with ratio Fe/Pt = 10 and ratio $NH_4Cl/(Pt+Fe) = 2$ (d); voltammetries of the FePt EG-based electrolyte with ratio Fe/Pt = 2 and ratio $NH_4Cl/(Pt+Fe) = 2$ (e); comparison between the voltammetries obtained at different Fe/Pt ratios, from 25 to 2, in presence and absence of NH_4Cl (f).

the position of the current maxima considerably shifts depending on the voltage scan rate. These two aspects are symptom of a highly non-reversible reaction system.[54]

The electrolyte with $FeCl_3$ was characterized by a 50 mM concentration in ethylene glycol. The peaks obtained through cyclic voltammetry can be observed in Fig. 2b. The Fe(III) to Fe(II) reduction started (E_{onset}) around 0 V vs Pt and peaked (E_{peak}) around −0.4 V vs Pt, while the Fe(II) to Fe(0) reduction did not present a real peak and only the potential at which the reaction starts to take place (E_{onset}) could be identified: −1.6 V vs Pt. The small cathodic peak visible at −1.4 V can be probably related to adsorption of Fe (III) and Fe(II) species at the surface of the electrode.[40] The Fe(0) to Fe(II) oxidation presented a value of E_{onset} around −1.15 V vs Pt and a value of E_{peak} around −0.6 V vs Pt, while the Fe(II) to Fe(III) oxidation started around −0.2 V vs Pt and peaked around 0.15 V vs Pt. The obtained values were found to be in line with those reported by Panzeri et al.[40] In analogy with the Pt containing electrolyte, also the Fe-containing one showed signs of hydrogen or oxygen evolution at high potentials. This is indicative of electrochemical decomposition of the water impurities introduced with the Fe salt.

Regarding the FePt electrodeposition bath, three different formulations were characterized through cyclic voltammetry. In particular, Fig. 2c refers to the scan in a solution 2 mM K_2PtCl_6 + 50 mM $FeCl_3$, Fig. 2d to the scan in 5 mM K_2PtCl_6 + 50 mM $FeCl_3$ + 110 mM NH_4Cl and Fig. 2e to the scan in 20 mM K_2PtCl_6 + 40 mM $FeCl_3$ + 120 mM NH_4Cl. Thanks to the previous voltammetries, performed in separate solutions of K_2PtCl_6 and $FeCl_3$, it was possible to attribute the peaks appearing in the three analyses. In

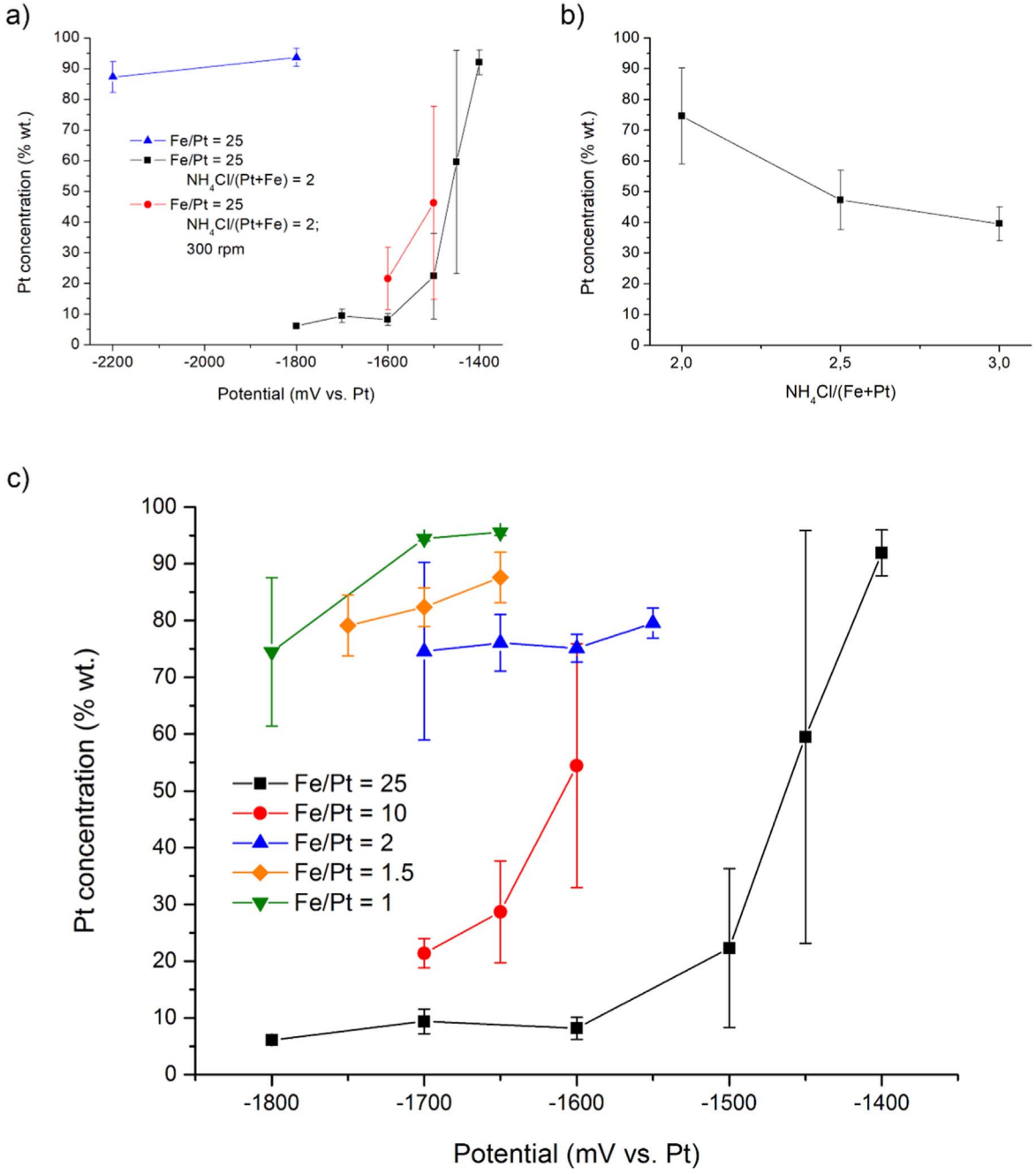

Figure 3. Effect of different deposition potentials on Pt concentration in the final FePt layer in absence or presence of NH_4Cl and in absence or presence of stirring (a); effect of different NH_4Cl/(Pt+Fe) ratios on Pt concentration in the final FePt layer at Fe/Pt = 2 and −1700 mV as deposition potential (b); effect of different deposition potentials on Pt concentration in the final FePt layer with respect to Fe/Pt ratio and at NH_4Cl/(Pt+Fe) = 2 (c).

Table II. Composition and thickness of some selected FePt deposits.

Sample	$FeCl_3$ [mM]	K_2PtCl_6 [mM]	NH_4Cl [mM]	NH_4Cl ratio	Potential [mV]	Time [s]	Pt [% at]	Thickness [nm]
FePt 1	40	20	180	3	−1650	1800	51.9	650
FePt 2	40	20	120	2	−1700	1800	58.4	240
FePt 3	40	20	150	2.5	−1600	1800	56.6	460
FePt 4	40	20	180	3	−1625	9730	51.1	1200
FePt 5	30	20	100	2	−1700	1800	59.3	200
FePt 6	30	20	100	2	−1750	1800	57.0	260
FePt 7	30	20	100	2	−1700	10800	44.0	3900
FePt 8	30	20	100	2	−1700	10800	53.2	4600

general, the characteristic peaks for Fe are always visible (reduction from Fe(III) to Fe(II), from Fe(II) to Fe(0) and oxidation from Fe(0) to Fe(II)). Also the Pt(II) to Pt(0) reduction is always evident, while the Pt(IV) to Pt(II) reduction appears, in all the case, superimposed to the Fe(III) to Fe(II) reduction. Moving from the voltammetry in Figs. 2c–2e, the total concentration of ions in solutions increased, the electrolyte became therefore more conductive and the registered mean current densities reached higher values.

The influence of NH_4Cl on the electrochemical behaviour of the electrolyte can be highlighted by directly overlapping (Fig. 2f) the voltammetric scans obtained with a scan rate of 50 mV s^{-1} in the solution 2 mM K_2PtCl_6 + 50 mM $FeCl_3$ (Fe/Pt ratio equal to 25) and in the solution 5 mM K_2PtCl_6 + 50 mM $FeCl_3$ + 110 mM NH_4Cl (Fe/Pt ratio equal to 10). The presence of NH_4Cl seems to partially inhibit the deposition of Pt and to favour that of Fe. Indeed, as can be seen in Fig. 2f, the cathodic peak corresponding to the reduction of Pt(II) to Pt(0) results less intense despite the highest Pt concentration (5 mM instead of 2 mM), while the peak of Fe deposition is shifted toward less negative potentials. This last effect can be attributed to a different complexation state of iron ions in solution.[45] The onset of the cathodic peaks related to Pt deposition is in all cases at around −0.8 V vs Pt, value that coincides with that obtained from the voltammetry in the solution of K_2PtCl_6. For the solutions containing NH_4Cl, however, the intensity of the peak is lower. Another important effect, related to the concentration of Pt ions, can be highlighted overlapping also the behaviour of the solution 20 mM K_2PtCl_6 + 40 mM $FeCl_3$ + 120 mM NH_4Cl electrolyte (Fe/Pt ratio equal to 2 and NH_4Cl/(Pt+Fe) ratio equal to 2) in Fig. 2f. It can be observed that, by increasing the concentration of Pt from 5 to 20 mM, a strong amplification of the Pt(II)/Pt(0) peak with respect to the Fe(II)/Fe(0) feature can be observed. This indicates a significant enhancement of mass transfer for Pt deposition.

Potentiostatic FePt electrodeposition tests.—The voltammetric tests carried out demonstrated that Fe and Pt can codeposit in EG-based solutions and that NH_4Cl could potentially have an important role in controlling the amount of Pt codeposited in the final alloy. As following step for the experimentation, potentiostatic deposition of FePt was attempted. Different bath formulations and electroplating operating conditions have been tested in order to find those providing an equiatomic composition of the deposit and a high compositional uniformity all over the plated surface. The measures to determine composition and thickness of the deposits were realized through XRF. For each sample, five measurements in five different points of the plating area (Fig. S3) were performed. The bars reported in Fig. 3 for each point represents the standard deviation calculated from these five composition values. Such standard deviation is representative of the compositional uniformity of the FePt.

In Fig. 3a, the effect of NH_4Cl on the content of platinum in the deposit is illustrated. The blue and black curves in the chart refer to a solution 2 mM K_2PtCl_6 + 50 mM $FeCl_3$ in ethylene glycol, respectively without NH_4Cl and with a concentration of 104 mM of NH_4Cl (for a (NH_4Cl/(Pt+Fe) ratio equal to 2). As expected, in both cases by decreasing the electroplating potential the amount of deposited iron increases, since this metal is less noble than platinum and therefore requires lower potentials to be reduced. In the case of the NH_4Cl free electrolyte, considering the large difference between the reduction potentials of the two metals, the concentration of Pt ions was kept low (at 2 mM, with a Fe/Pt ratio equal to 25). Despite of this precaution, almost only platinum deposited even at very low potentials. Considering the homologous NH_4Cl additivated solution, above −1400 mV basically only platinum deposited. This result is coherent with the position in the voltammetries of the reduction peak of Pt (II), which has its maximum at −1250 mV and continues developing at lower potentials. However, below −1400 mV, Fe started to efficiently codeposit with Pt. As demonstrated by the voltametric tests carried out, the presence of NH_4Cl determines a movement of the iron deposition onset towards higher potentials, the difference between reduction potentials of the two metals decreases and, consequently, the co-deposition becomes easier.

Another important parameter in the electroplating process is the stirring. In Fig. 3a the red curve refers to the electrodeposition from a solution 2 mM K_2PtCl_6 + 50 mM $FeCl_3$ + 104 mM NH_4Cl in ethylene glycol, like in the case of the black curve, with the addition of stirring at 300 rpm. As can be seen, the deposition of platinum is favoured under stirring conditions. This is due to a decrease in the thickness of the diffusion layer and therefore to an enhancement in the deposition of the most noble metal, which is evidenced by a translation of the deposition curve towards lower potentials. Furthermore, a considerable improvement in the uniformity of the samples was observed under stirring conditions. Observing the data for concentrations of Pt in the deposit around 50%, a great variability can be noticed, which means that the alloy composition varies a lot across the area of the sample. This can be explained from the low concentration of platinum ions in solution (2 mM).

Concerning the composition of the plating solution, another fundamental aspect is the ratio between the concentration of iron and platinum salts. In Fig. 3c, the effect of changes in this ratio is evaluated keeping constant the one between NH_4Cl and the two metallic salts. Moving from the black curve to the green one the Fe/Pt decreases and, when this happens, the amount of deposited platinum increases. Moreover, when the Fe/Pt ratio is low, the composition becomes highly Pt-rich and relatively independent from the potential applied. This is a direct consequence of the strong enhancement in mass transport for Pt evidenced in Fig. 2f. Finally, also the compositional uniformity of the coating increases when low Fe/Pt ratios are employed. As a result, compositionally uniform FePt layer were deposited at Fe/Pt ratios between 1.5 and 2.

It is possible to consider separately the increase of the ratio between the concentration of NH_4Cl and the concentration of metallic salts (Fig. 3b). By increasing this ratio, the concentration of platinum in the deposit decreases. This effect is highlighted by the data reported in Fig. 3b, which refer to a constant value of Fe/Pt equal to 2 and a deposition potential equal to −1700 mV. Finally, an important parameter to consider is the distance between the reference electrode and the cathode. Because of the high viscosity and the relatively low conductivity of the electrolyte, this distance must be reduced as much as possible and, above all, must be perfectly constant in all the tests.

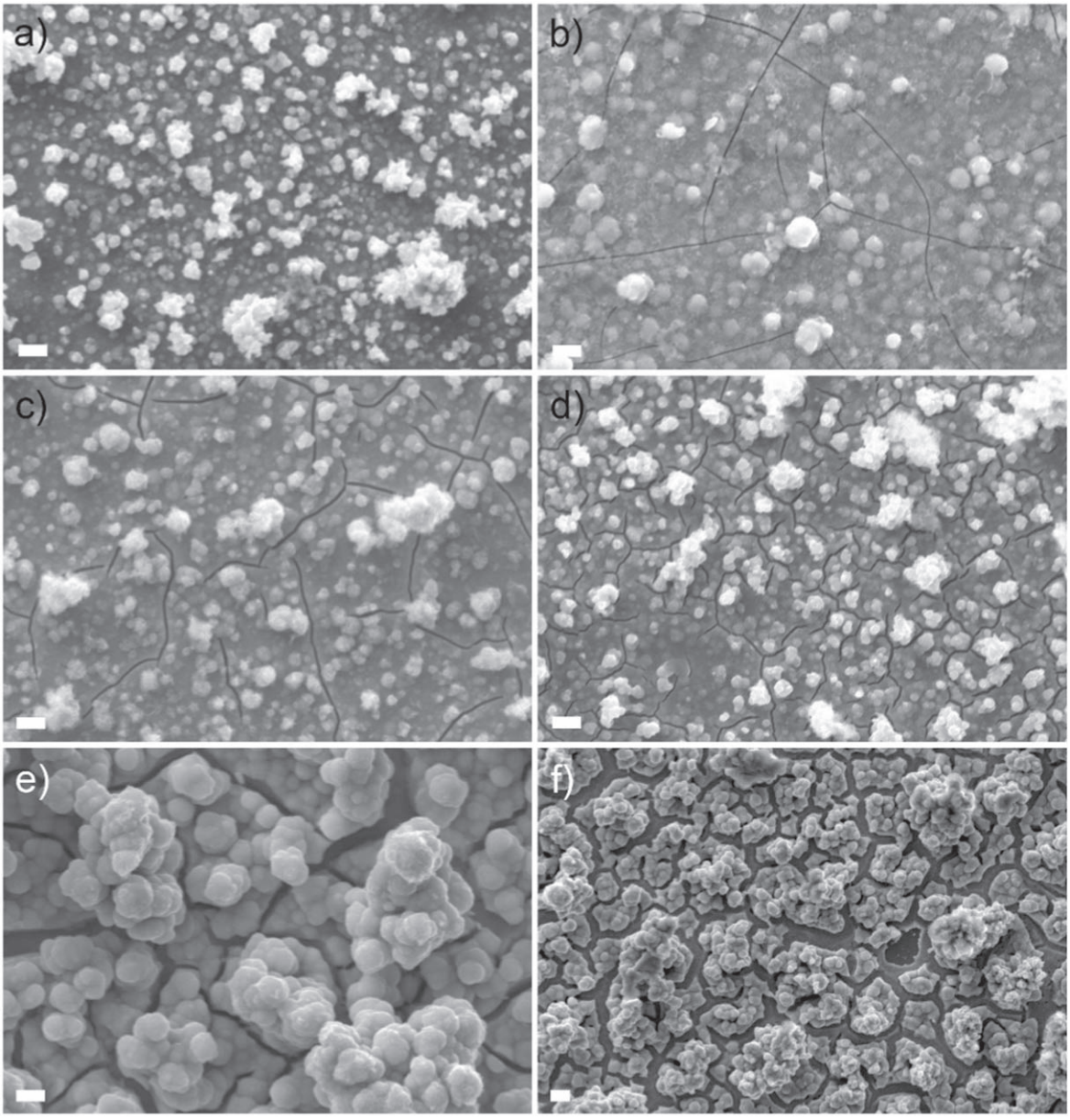

Figure 4. SEM morphology of some FePt layers: FePt 2 (a), FePt 3 (b), FePt 1 (c), FePt 6 (d), FePt 4 (e) and FePt 8 (f).

This preliminary characterisation was fundamental in order to define a meaningful range of values, for all the plating parameters, in which to perform the final tests. By looking at Fig. 3, it can be seen that the most promising conditions were: a Fe/Pt ratio between 2 and 1.5, a NH_4Cl/(Fe+Pt) ratio between 3 and 2, a moderate stirring and a potential range between −1600 mV and −1700 mV vs Pt. By operating in these conditions, the process was optimized and layers with an almost equiatomic composition were obtained.

Some deposits having a composition close to desired one were plated using the range of parameters defined and characterized in a complete way, yielding the results visible in Table II. The composition of each sample was thoroughly assessed through an EDS analysis along the thickness through profilometry. Among the listed samples, FePt 1, FePt 4, FePt 6, FePt 7 and FePt 8 underwent an annealing step at 600 °C.

Electrodeposited FePt morphological characterisation.—The surface of FePt layers was characterized through SEM analysis. Figures 4a, 4b, 4c, 4d and 4e refer respectively to samples FePt 2, FePt 3, FePt 1, FePt 6 and FePt 4 before annealing. Figure 4f, instead, depicts the surface of sample FePt 8 after annealing.

Samples obtained from depositions times of 30 min were characterized by a compact surface with granular outgrowths and hairline cracks. Longer electroplating times led to more cracked layers, as one can notice from samples FePt 8 (10800 s) and FePt 4 (9730 s). In these cases, the deposits formed a layer with a good compactness, covered by a more inhomogeneous and fractured one. As can be seen from Fig. 4f, after the annealing treatment the surface morphology did not change much and it appeared slightly more flacked and the cracks resulted enlarged.

Another important parameter to consider is the content of oxygen in the electroplated layers. For example, the amount of O in the as-deposited FePt 8 sample, calculated through an EDS analysis, was equal to 8.4% wt (34.6% at). Probably, the water impurities introduced by the two metallic salts lead to oxygen incorporation in the final coating. This effect can be observed also in water-based electrolytes. For example, Cherevko et al., with an aqueous electrolyte and for values of the current density comparable to those used in

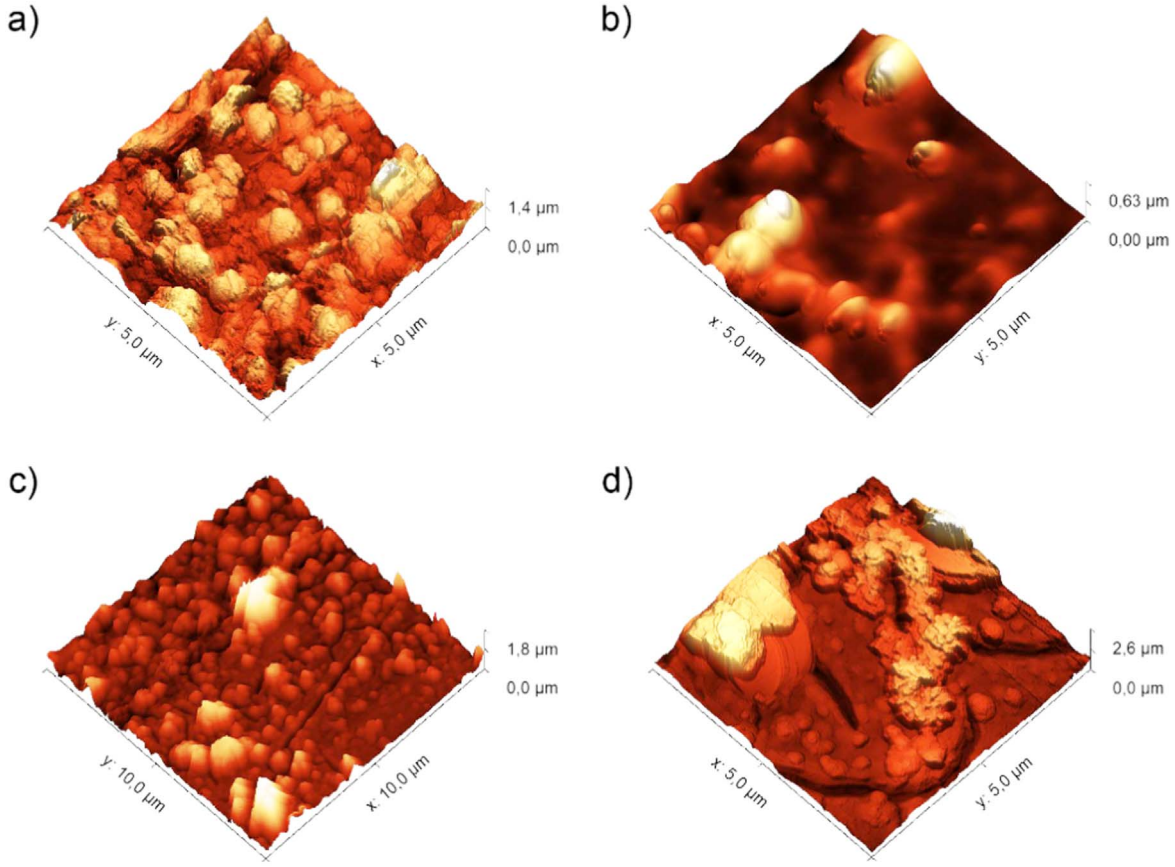

Figure 5. AFM morphology of some FePt layers: FePt 2 (a), FePt 3 (b), FePt 6 (c) and FePt 1 (d).

the present work, obtained an oxygen content equal to 40% at in FePt alloy films deposited at 65 °C and equal to 50% at in FePt films deposited at room temperature.[44] After the annealing in reducing H_2 atmosphere, the oxygen content of sample FePt 8 decreased, as expected, to very low values: 0.75% wt (3.5% at).

The roughness and the topography of the samples were investigated by performing an AFM analysis. In Fig. 5, for the samples FePt 2 (Fig. 5a), FePt 3 (Fig. 5b), FePt 6 (Fig. 5c) and FePt 1 (Fig. 5d), three-dimensional diagrams of areas of 5 μm × 5 μm or 10 μm × 10 μm are reported.

The mean roughness (R_a), calculated on areas of 10 μm × 10 μm, is reported in Table III. The highest value of R_a (284.4 nm) was reached by sample FePt 8, which is also the thickest and most cracked one.

Electrodeposited FePt phase composition.—A XRD analysis was performed to determine the crystalline phases present in the deposits and to confirm the formation of the ordered $L1_0$ phase after annealing. As deposited FePt is characterized by the presence of a partially disordered face-centered cubic (fcc) structure, where Fe and Pt atoms interchangeably occupy the fcc lattice positions (Fig. 6a). Upon annealing, the fcc phase evolves into the $L1_0$ phase, which is responsible for the high magnetic properties of the alloy. Indeed, it is characterized by a highly magneto-crystalline anisotropic face centered tetragonal (fct) structure.[55] As visible in the scheme reported in Fig. 6c, $L1_0$ is characterized by the alternance of planes containing mainly Fe atoms or Pt atoms. This structural peculiarity is the main source of magnetic anisotropy in the alloy.

In Fig. 6 it is possible to see, for samples FePt 8 (Figs. 6c and 6d) and FePt 6 (Figs. 6c and 6d), a comparison between the pattern recorded before and after the annealing step. Pre- and post-annealing data have been acquired also for the FePt 4 sample (Figs. S4 and S5). The gold peaks correspond to the substrate and therefore remain unchanged in all patterns. For all the three samples, the analysis of the as-deposited material showed the presence of only one phase, apart from gold: the partially disordered face-centered cubic (fcc) structural form of FePt. Owing to the annealing process at 600 °C, this phase was partially converted into the one of interest, the $L1_0$ phase. Indeed, in all the post-annealing images, the peaks corresponding to the $L1_0$ phase were clearly visible. After the treatment, the appearance of the (001), (110), (111), (200), (002), and (201) diffraction peaks of the $L1_0$ phase and the coexistence of fcc-FePt peaks indicated a partial phase transformation. This result is in agreement with other works where FePt is annealed at comparable temperatures.[4] Samples FePt 4 and FePt 8 had a composition closer to the desired one, respectively equal to 51.1% at Pt and 53.2% at Pt. In these two cases, the peaks corresponding to the phase $L1_0$ had a good relative intensity. Sample FePt 6, instead, is composed by 57.0 at % of Pt and its spectrum showed $L1_0$ peaks with a much lower relative intensity (as visible in the direct comparison reported in Fig. 6d). Therefore, as expected, the amount of $L1_0$ phase formed after the annealing step is strongly related to the composition of the deposited material: the closer is the alloy to be equiatomic, the greater will be the amount of desired phase formed (at the same annealing temperature).

Electrodeposited FePt magnetic characterisation.—In virtue of the phases observed via XRD, the annealed FePt samples hereby presented were expected to have a high coercivity. By using VSM, it was possible to measure the hysteresis loop for the samples of interest. Figure 7a refers to sample FePt 2, Fig. S6 to sample FePt 5, Fig. S7 to sample FePt 4 and Fig. 7b to sample FePt 1. Figure 7c is a direct comparison between samples FePt 7 and FePt 8.

In Table III the values of remanence B_R and coercivity H_C obtained from all the samples are presented. The three samples FePt 2, FePt 3 and FePt 5 were not annealed: as can be seen from their

Table III. Roughness and magnetic properties of some selected FePt deposits.

Sample	Pt [at %]	Thickness [nm]	Mean R_a [nm]	H_C in plane [Oe]	H_C out of plane [Oe]	Normalized B_R in plane	Normalized B_R out of plane	B_S [emu/cm^3]
FePt 1	51.9	650	265.1	1167	2556	0.55	0.29	283.2
FePt 2	58.4	240	120.8	142	210	0.21	0.08	138.4
FePt 3	56.6	460	124	100	187	0.15	0.06	100.4
FePt 4	51.1	1200	188.6	833	3001	0.55	0.33	318.3
FePt 5	59.3	200	86.4	250	300	0.18	0.15	160.1
FePt 6	57.0	260	155	1062	3500	0.60	0.38	309.5
FePt 7	44.0	3900	197.9	3875	4858	0.58	0.47	256.9
FePt 8	53.2	4600	284.4	10333	9888	0.71	0.6	289.1

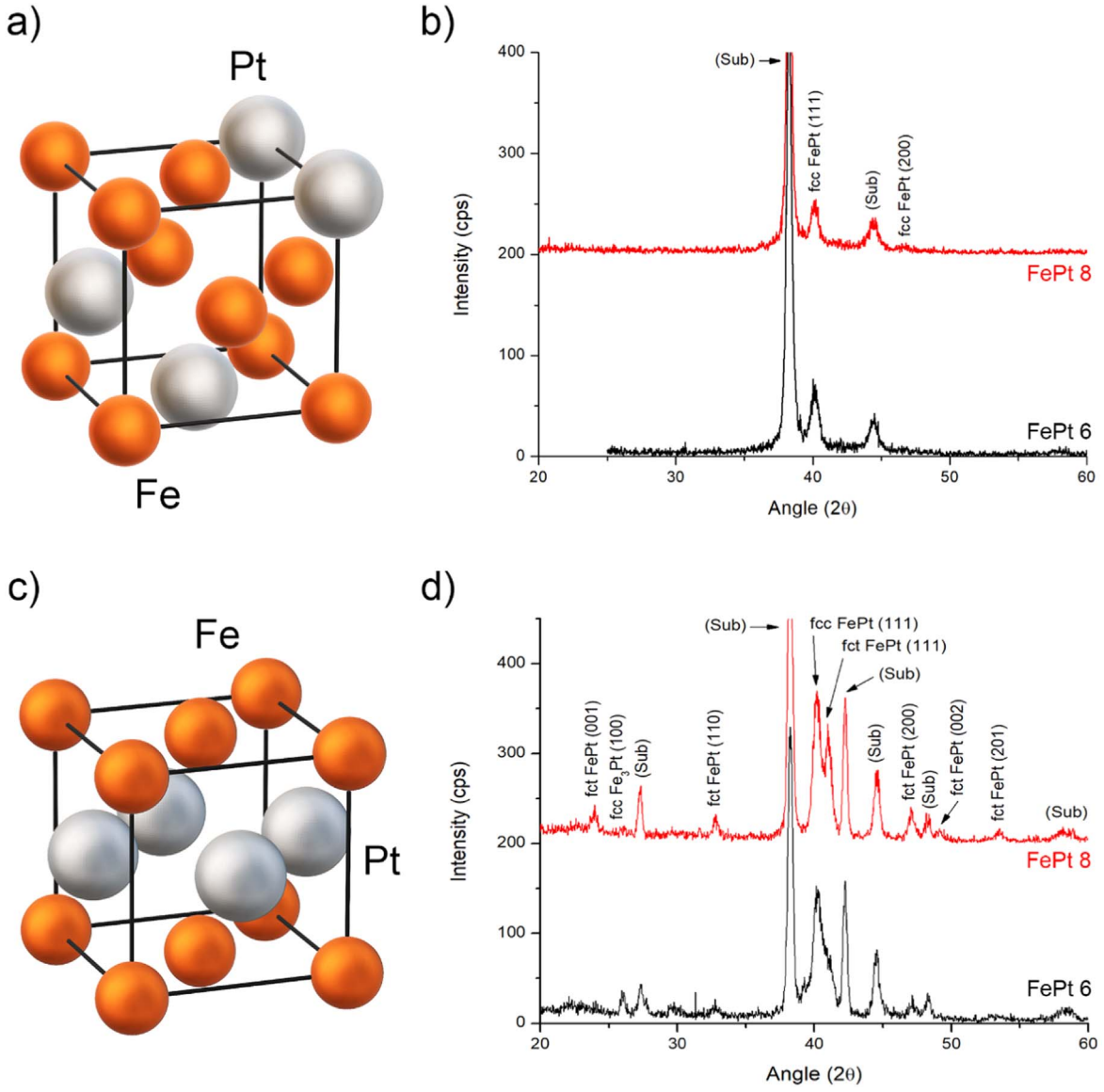

Figure 6. Crystalline structure of fcc FePt (a); XRD graphs of samples FePt 8 and FePt 6 before annealing (b); crystalline structure of fct FePt (c); XRD graphs of samples FePt 8 and FePt 6 after annealing (d).

hysteresis loops, their remanence and coercivity were very low, which is typical of soft ferromagnetic materials. This is a consequence of their fcc structure. Samples FePt 1, FePt 4, FePt 6, FePt 7 and FePt 8 underwent the annealing step, during which a fraction of ordered $L1_0$ phase formed. Indeed, their hysteresis loops showed good magnetic properties, which are in line with those reported in the literature. In particular, sample FePt 8 reached a coercivity of 10 kOe, which is comparable to the value obtained by Thongmee et al. after annealing in the same conditions employed by us (600 °C in reducing atmosphere, on gold substrate).[13] In our case, the highest coercivity was shown by this sample, FePt 8, which also had an almost equiatomic composition and was characterized by an extended formation of $L1_0$ phase during the annealing. Therefore, as expected, the hard ferromagnetic behaviour of FePt was strongly related to the amount of $L1_0$ phase in the material, which in turn was related to the composition obtained after the electrodeposition. The peculiar constricted appearance of the hysteresis cycles acquired from the annealed samples (e.g. Fig. 7c), which present a shoulder, is another direct consequence of the coexistence of the soft magnetic fcc phase and the hard magnetic $L1_0$ phase in the coatings.[4]

The effect of alloy composition on the magnetic properties after annealing is clearly visible in the direct comparison between FePt 7 and FePt 8 reported in Fig. 7c. The coercivity of the non-equiatomic sample (FePt 7) was only 37.5% of the value for the equiatomic one (in plane). Concerning saturation magnetization B_S, values were found to be in the hundreds emu cm^{-3} range[56] and higher in annealed FePt samples (Table III). This was expected, since the annealing process in hydrogen-containing atmosphere reduced the oxides present in the layers.[57]

Conclusions

In the present work, the electrodeposition of equiatomic FePt from a non-aqueous solution based on ethylene glycol as solvent was studied. Unlike most previous studies, a trivalent iron salt was employed in combination with a tetravalent platinum salt. In addition, ammonium chloride was employed as additive to tune the codeposition of the two metals, obtaining thus a reproducible and uniform composition over the surface of the samples deposited. The electrochemical characterization carried out clearly demonstrated the

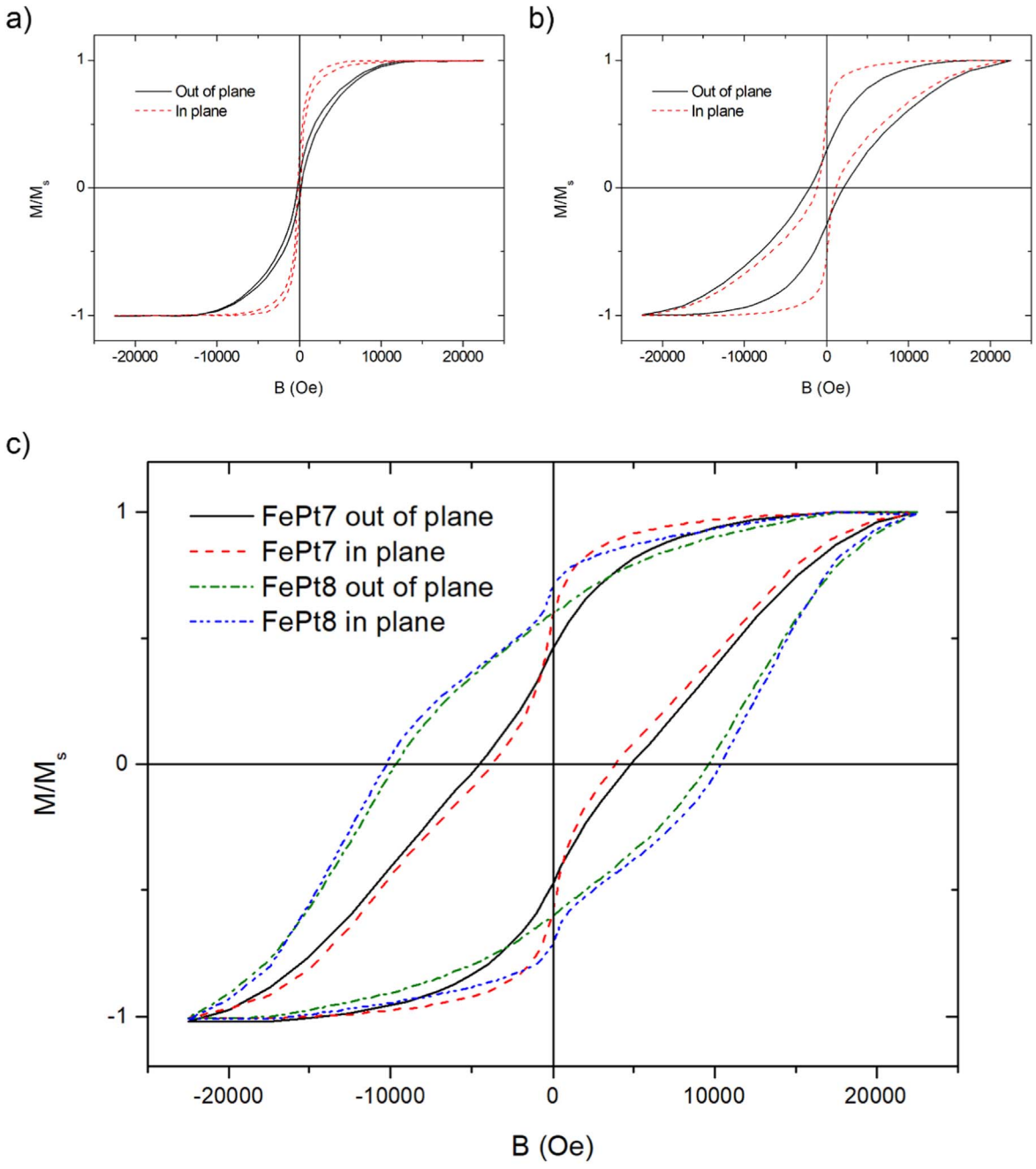

Figure 7. VSM of sample FePt 2 (a) and FePt 1 (b); comparison between the VSM graphs of samples FePt 7 and FePt 8 (c).

effective reduction and codeposition of iron and platinum and the relevant effect of ammonium chloride on the composition of the resulting alloy. Indeed, the additive increased electrolyte conductivity and strongly favored iron codeposition at low potentials. Optimized bath composition and working conditions were successfully individuated and nearly equiatomic FePt alloys were easily deposited, with thicknesses up to few microns, from electrolytes characterized by Fe/Pt ratios between 1.5 and 2 and NH_4Cl/(Fe+Pt) ratios between 2 and 3. Morphological analysis demonstrated the comparatively high purity of the deposits as well as their cracked morphology. From the phase composition point of view, as-deposited FePt layers were characterized by the presence of a moderately ordered fcc structure, which partially evolved into the highly magneto-crystalline anisotropic $L1_0$ phase after annealing at 600 °C. As expectable, the percentage of $L1_0$ phase visibly depended on the composition of the alloy. Finally, the magnetic characterization carried out evidenced that it was possible to obtain attractive hard-magnetic properties from the FePt layers by limiting the annealing temperature to relatively low values. In particular, a remanence higher than 10 kOe was reached after annealing at 600 °C. In front of this promising result, some aspects of FePt deposition from EG based solutions requires further experimentation to be fully understood. These include, for example, the influence of magnetic domains organization and evolution in the layers on final FePt coercivity and remanence. In addition, the influence of a cracked morphology like the one observed on the magnetic properties should be the subject of future studies. From this point of view, crack suppression methodologies can be applied to mitigate cracks formation and to evaluate the magnetic properties of crack-free layers. A typical example for such methodologies is pulse reverse electrodeposition, which can efficiently limit hydrogen adsorption and consequently can decrease embrittlement phenomena.

ORCID

Roberto Bernasconi https://orcid.org/0000-0003-2193-8017
Luca Magagnin https://orcid.org/0000-0001-5553-6441

References

1. D. Ho, X. Sun, and S. Sun, *Acc. Chem. Res.*, **44**, 875 (2011).
2. K. Leistner, J. Thomas, H. Schlörb, M. Weisheit, L. Schultz, and S. Fähler, *Appl. Phys. Lett.*, **85**, 3498 (2004).
3. M. Toda, H. Xu, and T. Ono, *Phys. Status Solidi Appl. Mater. Sci.*, **218**, 6 (2021).
4. Y. Ying, H. Wang, J. Zheng, J. Yu, W. Li, L. Qiao, W. Cai, and S. Che, *J. Supercond. Nov. Magn.*, **33**, 3563 (2020).
5. J. C. Lodder and L. T. Nguyen, *Encyclopedia of Materials: Science and Technology* (Elsevier, Amsterdam) p. 1 (2005).
6. S. Sun, C. B. Murray, D. Weller, L. Folks, and A. Moser, *Science*, **287**, 1989 (2000).
7. J. Chen, C. Sun, and G. M. Chow, *Mater. Sci.*, **5**, 238 (2008).
8. Y. Shi, M. Lin, X. Jiang, and S. Liang, *J. Nanomater.* (2015).
9. V. M. Kadiri, J.-P. Günther, S. N. Kottapalli, R. Goyal, F. Peter, M. Alarcón-Correa, K. Son, H.-N. Barad, M. Börsch, and P. Fischer, *Eur. Phys. J. E*, **44**, 1 (2021).
10. P. Mokhtari, P. Kameli, M. H. Ehsani, A. S. Esmaeily, H. Kalhori, and H. Salamati, *J. Supercond. Nov. Magn.*, **30**, 1949 (2017).
11. I. Matsui, *J. Nanoparticle Res.*, **8**, 429 (2006).
12. L. Zhang, W. W. Zhong, S. S. Yu, S. X. Xue, Y. P. Liu, Z. G. Li, and W. P. Chen, *J. Alloys Compd.*, **560**, 177 (2013).
13. S. Thongmee, J. Ding, J. Y. Lin, D. J. Blackwood, J. B. Yi, and J. H. Yin, *J. Appl. Phys.*, **101**, 09K519 (2007).
14. S. Ichihara, M. Ueda, and T. Den, *Intermag ASIA 2005 Dig. IEEE Int. Magn. Conf.*, **41**, 179 (2005).
15. F. M. F. Rhen and J. M. D. Coey, *J. Magn. Magn. Mater.*, **322**, 1572 (2010).
16. A. P. Abbott and K. J. McKenzie, *Phys. Chem. Chem. Phys.*, **8**, 4265 (2006).
17. F. Endres, A. Abbott, and D. MacFarlane, *Electrodeposition from Ionic Liquids* (Wiley, New York, NY) (2017).
18. F. Liu, Y. Deng, X. Han, W. Hu, and C. Zhong, *J. Alloys Compd.*, **654**, 163 (2016).
19. M. U. Ceblin, S. Zeller, B. Schick, L. A. Kibler, and T. Jacob, *Chem. Electro. Chem*, **6**, 141 (2019).
20. R. Bernasconi, A. Lucotti, L. Nobili, and L. Magagnin, *J. Electrochem. Soc.*, **165**, D620 (2018).
21. M. F. Rahman, R. Bernasconi, and L. Magagnin, *J. Optoelectron. Adv. Mater.*, **17**, 122 (2015).
22. X. Cao, L. Xu, C. Wang, S. Li, D. Wu, Y. Shi, F. Liu, and X. Xue, *Coatings*, **10**, 1154 (2020).
23. M. Amiri and D. Bélanger, *Chem. Electro. Chem*, **8**, 2737 (2021).
24. H. F. Alesary, S. Cihangir, A. D. Ballantyne, R. C. Harris, D. P. Weston, A. P. Abbott, and K. S. Ryder, *Electrochim. Acta*, **304**, 118 (2019).
25. A. Y. M. Al-Murshedi, J. M. Hartley, A. P. Abbott, and K. S. Ryder, *Trans. IMF*, **97**, 321 (2019).
26. J. A. Juma, *Arab. J. Chem.*, **14**, 103036 (2021).
27. L. Vieira, J. Burt, P. W. Richardson, D. Schloffer, D. Fuchs, A. Moser, P. N. Bartlett, G. Reid, and B. Gollas, *Chemistry Open*, **6**, 393 (2017).
28. G. Panzeri, M. Tresoldi, C. Rinaldi, and L. Magagnin, *J. Electrochem. Soc.*, **164**, D930 (2017).
29. S. P. Rosoiu, S. Costovici, C. Moise, A. Petica, L. Anicai, T. Visan, and M. Enachescu, *Electrochim. Acta*, **398**, 139339 (2021).
30. M. Manolova, R. Böck, I. Scharf, T. Mehner, and T. Lampke, *J. Alloys Compd.*, **855**, 157462 (2021).
31. X. Xu, S. Sturm, J. Zavasnik, and K. Z. Rozman, *Chem. Electro. Chem*, **6**, 2860 (2019).
32. A. Liu, Z. Shi, and R. G. Reddy, *Ionics*, **26**, 3161 (2020).
33. S. P. Rosoiu, A. G. Pantazi, A. Petica, A. Cojocaru, S. Costovici, C. Zanella, T. Visan, L. Anicai, and M. Enachescu, *Metals*, **10**, 1455 (2020).
34. F. I. Danilov, A. A. Kityk, D. A. Shaiderov, D. A. Bogdanov, S. A. Korniy, and V. S. Protsenko, *Surf. Eng. Appl. Electrochem.*, **55**, 138 (2019).
35. J. Winiarski, A. Niciejewska, J. Ryl, K. Darowicki, S. Baśladyńska, K. Winiarska, and B. Szczygieł, *Materials*, **13**, 924 (2020).
36. R. Li, Q. Chu, and J. Liang, *RSC Adv.*, **5**, 44933 (2015).
37. A. M. P. Sakita, R. Della Noce, A. V. Benedetti, J. Garcia-Amoros, and E. Valles, *J. Electrochem. Soc.*, **165**, D266 (2018).
38. A. Lahiri and F. Endres, *J. Electrochem. Soc.*, **164**, D597 (2017).
39. R. Bernasconi, G. Panzeri, G. Firtin, B. Kahyaoglu, L. Nobili, and L. Magagnin, *J. Phys. Chem. B*, **124**, 10739 (2020).
40. G. Panzeri, A. Accogli, E. Gibertini, C. Rinaldi, L. Nobili, and L. Magagnin, *Electrochim. Acta*, **271**, 576 (2018).
41. Z. Hong-ru, Y. Yun-dan, W. Guo-ying, and G. Hong-liang, *Int. J. Electrochem. Sci.*, **7**, 5544 (2012).
42. G. Wei, H. Zhou, H. Ge, and H. Dettinger, *Surf. Eng.*, **32**, 344 (2016).
43. K. Leistner, P. Schaaf, A. Voss, S. Fähler, L. Schultz, and H. Schlörb, *Electrochim. Acta*, **53**, 6973 (2008).
44. S. Cherevko, J. Fu, K. Y. Song, and C. H. Chung, *Korean J. Chem. Eng.*, **26**, 1766 (2009).
45. S. Fashu, C. D. Gu, J. L. Zhang, M. L. Huang, X. L. Wang, and J. P. Tu, *Trans. Nonferrous Met. Soc. China (English Ed.)*, **25**, 2054 (2015).
46. P. E. Valverde, T. A. Green, and S. Roy, *J. Appl. Electrochem.*, **50**, 699 (2020).
47. M. Bučko, S. Roy, P. Valverde-Armas, A. Onjia, A. C. Bastos, and J. B. Bajat, *J. Electrochem. Soc.*, **165**, H1059 (2018).
48. Y. Cui, C. Li, J. Yin, S. Li, Y. Jia, and M. Bao, *Design, Synthesis and Properties of Acidic Deep Eutectic Solvents Based on Choline Chloride* (Elsevier) 236, p. 338 (2017).
49. A. P. Abbott, D. Boothby, G. Capper, D. L. Davies, and R. K. Rasheed, *J. Am. Chem. Soc.*, **126**, 9142 (2004).
50. A. Mahapatro and S. K. Suggu, *Adv. Mater. Sci*, **3**, 1 (2018).
51. P. He, H. Liu, Z. Li, and J. Li, *J. Electrochem. Soc.*, **152**, E146 (2005).
52. O. Diaz-Morales, T. J. P. Hersbach, C. Badan, A. C. Garcia, and M. T. M. Koper, *Faraday Discuss.*, **210**, 301 (2018).
53. E. Gómez and E. Vallés, *Int. J. Electrochem. Sci.*, **8**, 1443 (2013).
54. V. Climent and J. M. Feliu, *Encycl. Interfacial Chem. Surf. Sci. Electrochem.*, 48 (2018).
55. K. Son, G. Ryu, H. H. Jeong, L. Fink, M. Merz, P. Nagel, S. Schuppler, G. Richter, E. Goering, and G. Schütz, *Small*, **15**, 1 (2019).
56. J. Yu, T. Xiao, X. Wang, X. Zhou, X. Wang, L. Peng, Y. Zhao, J. Wang, J. Chen, H. Yin, and W. Wu, *Nanomaterials*, **9**, 1 (2019).
57. K. Leistner, J. Thomas, S. Baunack, H. Schlörb, L. Schultz, and S. Fähler, *J. Magn. Magn. Mater.*, **290–291**, 1270 (2005).